

# A Fiber Fluidic Nanogenerator Made from Aligned Carbon Nanotubes Composited with Transition Metal Oxide

Tiancheng Zhao, Yajie Hu, Wen Zhuang, Yifan Xu, Jianyou Feng, Peining Chen,\* and Huisheng Peng\*

Cite This: *ACS Materials Lett.* 2021, 3, 1448–1452

Read Online

ACCESS |



Metrics &amp; More

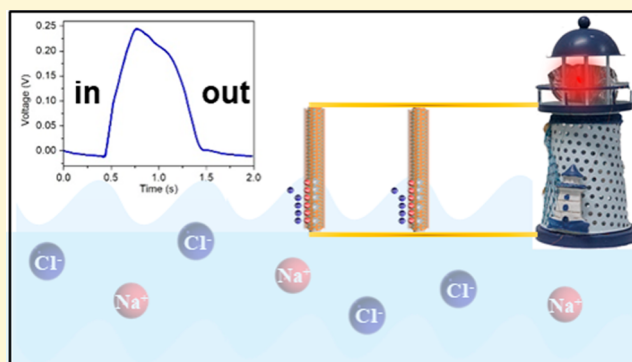


Article Recommendations



Supporting Information

**ABSTRACT:** Harvesting electricity from water has been recognized as an effective way to deal with the increasing energy shortage. The nanogenerators made from carbon nanomaterials have been widely studied to harvest energy from various forms of water. However, its electric generation is usually not sufficient for practical applications. Here, we develop a flexible fiber fluidic nanogenerator based on aligned carbon nanotube/transition metal oxide composite film. An open-circuit voltage of 0.31 V combined with an output power of 30 mW/m<sup>2</sup> had been produced when the fluidic nanogenerator was inserted into saline solution. The output power is superior to the majority of previous hydroelectric generators based on carbon nanomaterials. A stable output voltage of 1.8 V could be further achieved by connecting fiber generators in series. The enhanced electricity generation after introduction of transition metal oxides is attributed to the intensified charge unbalance at the interfacial electric double layer between the carbon nanotube and aqueous solution, which provides a new way for creating high-performing hydroelectric generators.



With the growing exhaustion of traditional fossil energy, the demand for renewable energy is increasingly urgent. Harvesting electricity from the mechanical or electrochemical energy stored in water has been recognized as an effective way to deal with the increasing energy shortage due to the abundance of water.<sup>1–3</sup> The utilization of hydropower through an electromagnetic generator based on large dams and water wheels has occurred for more than 100 years. Over the past decade, miniaturized and flexible nanogenerators that can efficiently collect energy from water/moisture movement have aroused increasing interest because of their great potential in wearable electronics.<sup>4–6</sup>

On the basis of the principles of interfacial interaction between carbon atoms and water molecules, the nanogenerators made from carbon nanomaterials have been developed to harvest energy from various forms of water such as flows,<sup>7–10</sup> waves,<sup>11–13</sup> drops,<sup>14,15</sup> and moisture.<sup>16,17</sup> Among them, macroscopic carbon nanotube (CNT) assemblies in forms of fiber and film can effectively maintain the unique properties of individual CNTs such as high mechanical strength, high electrical conductivity, and large specific surface area and are considered promising candidates for high-performing fluidic nanogenerators.<sup>7,10,12</sup> For instance, aligned CNT fibers could generate an electricity output of many tens

of millivolts with high power conversion efficiency,<sup>4,12</sup> caused by the unbalanced charges accumulated along the CNT fiber as inserted into aqueous solution. The working mechanism based on an electric double layer formed at the interface of aligned CNTs and water indicates that the electricity output could be enhanced by increasing the capacity of aligned CNTs for ion adsorption.<sup>4</sup> Transition metal oxides like ruthenium dioxide (RuO<sub>2</sub>) are widely used in energy storage devices due to their excellent electrochemical properties.<sup>18–23</sup> For instance, it is known that the introduction of transition metal oxides in the electrodes of supercapacitors can effectively improve electrochemical performance by increasing the capacity.<sup>24–28</sup> We hypothesized that if transition metal oxide is introduced into the aligned CNTs to fabricate a fluidic nanogenerator, it is possible to achieve high electricity generation from water movement.

Received: July 7, 2021

Accepted: August 30, 2021

In this work, we report a flexible fiber fluidic nanogenerator based on aligned CNT/transition metal oxide composite films. Ruthenium dioxide was chosen as a demonstration to be incorporated into the aligned CNTs using a dip-coating method. The electricity output could be tuned by changing parameters like insertion speed, solution concentration, ion species, content of  $\text{RuO}_2$ , etc. An output voltage of 0.31 V and a current of  $83 \mu\text{A}$  were generated from the resultant fluidic nanogenerators. The generated power output ( $30 \text{ mW/m}^2$ ) was superior to the majority of hydroelectric generators. It reveals that the charge unbalance in the electric double layer at the interface between the CNT/ $\text{RuO}_2$  and water during movement could efficiently enhance the capacity for ion absorption of CNT and thus induce higher electricity output than that without  $\text{RuO}_2$ .

Figure 1a schematically illustrates the fabrication process of the fluidic nanogenerator. The CNT sheet was continuously

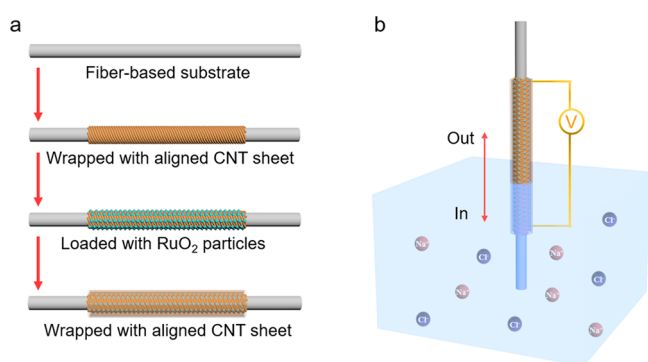


**Figure 1.** (a) Schematic illustration of preparation process of a fluidic nanogenerator. (b) Schematic illustration of the experimental setup to measure the electricity generation from the fluidic nanogenerator.

drawn from a spinnable CNT array synthesized by chemical vapor deposition, and then wrapped onto an elastic polymer fiber substrate. The CNTs were highly aligned in the sheet (Figure S1a, b). The transition metal oxides with particle sizes from  $\sim 10$  to  $90 \text{ nm}$  were then introduced into the CNT sheet (Figures S2, S3) via a dip-coating method to serve as active components for high electricity generation. The aligned structure of the CNT sheet was well maintained after the introduction of transition metal oxide particles.  $\text{RuO}_2$  with an average diameter of  $\sim 10 \text{ nm}$  (Figure S2) was demonstrated as a proof of concept. An additional layer of the CNT sheet was wrapped around the CNT/ $\text{RuO}_2$  composite film to stabilize  $\text{RuO}_2$  particles. This resultant composite layer had a typical thickness of around  $2 \mu\text{m}$  (Figure S4). The water contact angle of this composite layer ( $120.2^\circ$ ) is similar to that of the aligned CNT film (Figure S5), indicating the hydrophobicity surface was well maintained after the introduction of  $\text{RuO}_2$ . The hydrophobic surface of the fiber generator could effectively avoid solution retention (Figure S6 and Video S1) and thus make it repeatedly and stably generate electricity during cyclic inserting and pulling-out motions. Copper wires were connected to the two ends of the composite fiber for electricity measurements. The I–V curve of the composite fiber in air was linearly dependent, indicating a good ohmic contact between the copper wire and CNT layer (Figure S7). The generated voltage and current were traced to evaluate the performance of the fluidic nanogenerator.

The composite fiber could function as a fluidic nanogenerator to generate electricity when it was inserted into the saline water (Figure 1b). For instance, when the fluidic nanogenerator was inserted into the saline water with a speed of  $9.2 \text{ cm/s}$ , the generated open-circuit voltage was gradually increased to a peak value of  $\sim 0.25 \text{ V}$  (Figure 2a) and then

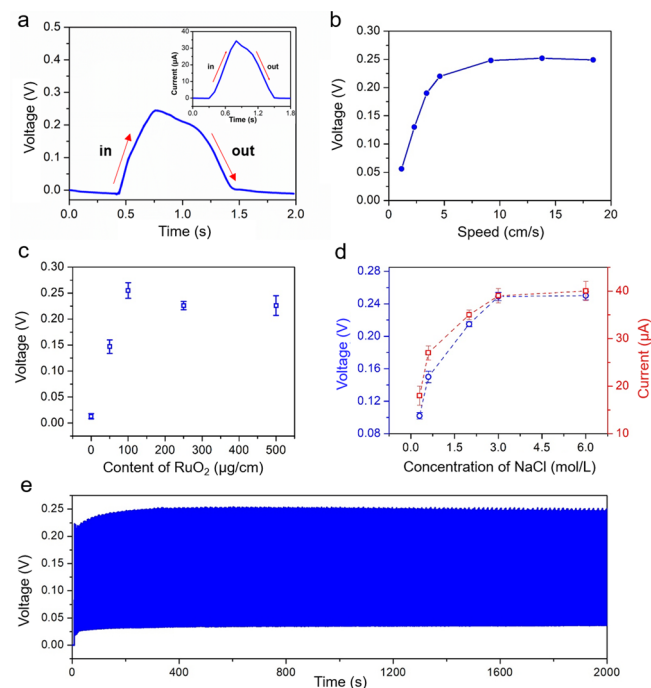


**Figure 2.** Electricity generation of the fluidic nanogenerator when inserted into and pulled out of the saline water. (a) Typical voltage signals and current signals produced during inserting and pulling out of the fiber generator. (b) Dependence of the output voltage on the insertion speed in a saturated NaCl solution. (c) Dependence of the output voltage on the content of  $\text{RuO}_2$  in a saturated NaCl solution (the insertion speed was  $13.8 \text{ cm/s}$ ). (d) Dependence of the output voltage and current on the concentration of NaCl solution (the insertion speed was  $13.8 \text{ cm/s}$  and the content of  $\text{RuO}_2$  was  $100 \mu\text{g/cm}$ ). (e) Output voltage generated by repeatedly inserting the fluidic nanogenerator into a saturated NaCl solution for 2000 s (the insertion speed was  $13.8 \text{ cm/s}$ ).

returned to the original state once the composite fiber was pulled out of the saline water. Similarly, a short-circuit current with a peak value of  $35 \mu\text{A}$  was generated after the insertion (Figure 2a). Note that the output voltage was influenced by the immersed length of the fluidic nanogenerator in the saline water. For instance, the voltage increased from 0.06 to 0.31 V with the immersed length increasing from 1 to 9 cm (Figure S8). For the convenience of discussion, the fluidic nanogenerator with a contact length of 5 cm was studied unless specified otherwise.

With the insertion speed increasing from 1.15 to  $9.2 \text{ cm/s}$  in a saturated NaCl solution, the output voltage increased from 0.056 to 0.25 V (Figure 2b). When the insertion speed further increased to  $18.4 \text{ cm/s}$ , the voltage remained nearly unchanged. The content of  $\text{RuO}_2$  was an important factor in influencing the performance of the fluidic nanogenerator. The fluidic nanogenerator without the addition of  $\text{RuO}_2$  generated a low voltage of 0.013 V, while the voltage value was significantly enhanced after the introduction of  $\text{RuO}_2$ . For

instance, the generated voltage reached 0.15 V when the content of RuO<sub>2</sub> was 50 μg/cm, which is 10 times higher than that generated by the counterpart without RuO<sub>2</sub> particles. A maximal value of output voltage (0.25 V) occurred with a content of 100 μg/cm (Figure 2c). Changing the concentration of saline water also affected the electricity generation. When the insertion speed was 13.8 cm/s and the content of RuO<sub>2</sub> remained 100 μg/cm, with the concentration of NaCl increasing from 0.3 to 6 mol/L, the output voltage increased from 0.1 V to a maximal value of 0.25 V. A similar trend of output current was also demonstrated with an increasing concentration of saline water (Figure 2d). Moreover, the open-circuit voltage was well maintained after repeated insertion for a long duration of 2000 s (Figure 2e), indicating that the fluidic nanogenerator exhibited good stability.

On the basis of the experimental results, a working mechanism is proposed in Figure 3a. The zeta potential of CNT/RuO<sub>2</sub> in deionized water was measured as a negative value, indicating a negatively charged surface of CNT/RuO<sub>2</sub> inclined to absorb Na<sup>+</sup> (Figure 3b), which is similar to CNTs without the introduction of RuO<sub>2</sub> as previously reported.<sup>4,12</sup> Similarly, the aligned CNTs composited with other transition

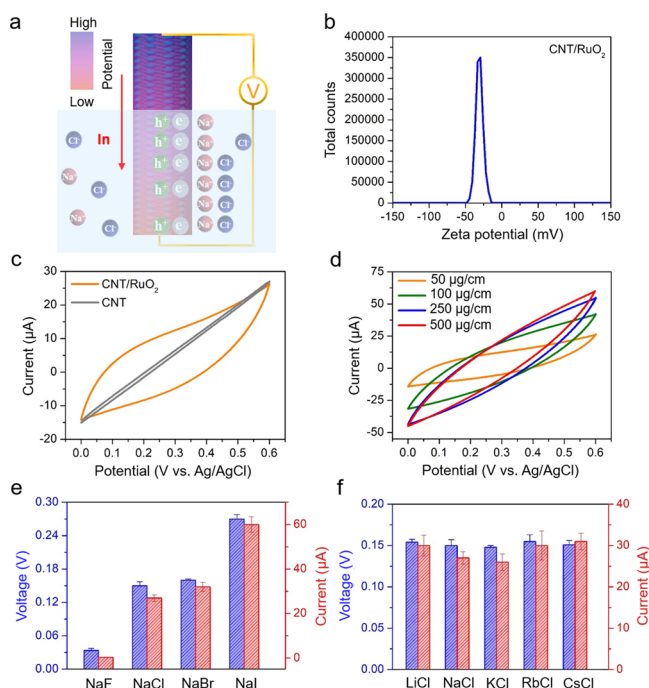


**Figure 3.** Mechanism of the fluidic nanogenerator. (a) Schematic illustration of the mechanism showing the flowing potential in the fluidic nanogenerator. An electric double layer is formed on the surface of the fluidic nanogenerator in the NaCl solution. Induced potential difference and hole concentration gradient in the fluidic nanogenerator are also illustrated. (b) Zeta potential of the CNT/RuO<sub>2</sub> in deionized water. (c) Cyclic voltammograms of the fluidic nanogenerator without and with RuO<sub>2</sub>. (d) Cyclic voltammograms of the fluidic nanogenerator with increasing RuO<sub>2</sub> contents. (e) Output voltages and currents produced during inserting and pulling out processes in NaF, NaCl, NaBr, and NaI solutions with the same concentration of 0.6 mol/L. (f) Output voltages and currents produced during inserting and pulling out processes in LiCl, NaCl, KCl, RbCl, and CsCl solutions with the same concentration of 0.6 mol/L. The RuO<sub>2</sub> content of the fiber fluidic nanogenerators was 100 μg/cm, and the immersed length of them in the solution was 5 cm in e and f.

metal oxides also demonstrated negatively charged surfaces (Figure S9). When the fluidic nanogenerator contacted NaCl solution, an electric double layer consisting of a stern layer formed by absorbing Na<sup>+</sup> and a diffusion layer full of counter Cl<sup>-</sup> ions would be formed at the interface between the composite fiber and NaCl solution. When the fluidic nanogenerator was inserted into the NaCl solution, Na<sup>+</sup> tends to be absorbed at the surface of the CNT/RuO<sub>2</sub> composite fiber, while Cl<sup>-</sup> in the diffusion layer was retarded in migration to counteract the net charge of the stern layer. Therefore, excessive positive charges attracted the electrons in CNT/RuO<sub>2</sub> to counteract the net charge, resulting in an increase of local hole concentration and further enhancement of potential, thus leading to a higher output voltage.

To further verify our mechanism, cyclic voltammograms of the fluidic nanogenerator in saturated NaCl solution was measured in a three-electrode electrochemical cell. No obvious cathodic or anodic peaks are observed in Figure 3c,d, indicating that the fluidic electricity generation process was related to the electric double layer formed at the interface of CNT/RuO<sub>2</sub> composite film and NaCl solution.<sup>1,4</sup> As shown in Figure 3c, due to the higher mass specific capacitance of RuO<sub>2</sub> than that of the aligned CNT sheet, the capacitance of the fluidic nanogenerator based on the CNT/RuO<sub>2</sub> composite film was significantly improved, which is consistent with the experimental result showing enhanced output voltage of the fluidic nanogenerator after the introduction of RuO<sub>2</sub> in the aligned CNTs. Furthermore, with increasing contents of RuO<sub>2</sub>, the capacitance increased and then remained nearly unchanged (Figure 3d), which is also consistent with the trend of voltage versus the content of RuO<sub>2</sub>. In other words, the higher capacitance might enable a larger capacity to absorb Na<sup>+</sup> and intensify the charge unbalance, thus leading to a higher output voltage. However, the voltage output could not be continuously improved by just increasing the RuO<sub>2</sub> content (Figure 3d), because the degree of charge unbalance is also limited by the other conditions like inserting speed, NaCl concentration, and type of the salt. As expected, the composite fiber incorporated with other metal oxides like MnO<sub>2</sub>, IrO<sub>2</sub>, NiO, and Co<sub>3</sub>O<sub>4</sub> could also generate obvious electricity (Figure S10). The fluidic nanogenerator composited with SiO<sub>2</sub> and polyaniline that is in favor of capacitance could also generate an enhanced electricity output (Figures S11 and S12). For practical applications, high electric generation can be possibly achieved by introducing other advanced active materials with high specific capacities.

According to the above proposed mechanism, the key to the voltage generation was that the anion could not immediately migrate to the interface to counteract the net charge. It is predicted that an anion with a larger radius could generate larger voltage while the radius of the cations would not affect the generated voltage value. As shown in Figures 3e and S13, when the fluidic nanogenerator was inserted into the solutions with different anions, higher electricity output was generated in those solutions containing larger anions. In comparison, the output voltage and current were nearly unchanged when the fluidic nanogenerator inserted into saline water containing different cations (Figure 3f). The experimental results are consistent with predictions based on the proposed mechanism, indicating the rationality of the proposed mechanism.

To study the output power of the fluidic nanogenerator under working conditions, output voltage and current were measured when the fluidic nanogenerator was connected to

different external resistances.<sup>12,29</sup> As shown in Figure S14, with the increase of external resistance, the output voltage increased while the output current decreased. At an external resistance of 4 k $\Omega$ , the output power reached a maximal value of 30 mW/m<sup>2</sup>, which is superior to the majority of hydroelectric generators reported previously (Figure 4a).<sup>6,13,30</sup>

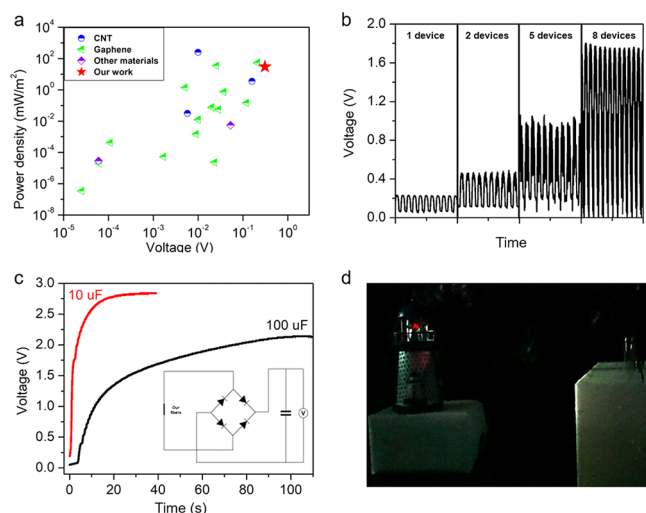


**Figure 4.** Demonstration of the fluidic nanogenerator as a practical power source. (a) The output voltage and power density of our fluidic nanogenerator in comparison to previous hydroelectric generators.<sup>6,13,30</sup> (b) Voltage output of fluidic nanogenerators connected in series. (c) Voltage–time curves of commercial capacitors charged by 11 fluidic nanogenerators connected in series. The inset is the charge storage circuit. A full-wave diode rectifier was used to avoid electricity leakage. (d) A conceptual lighthouse powered by the fluidic nanogenerators.

The output electricity of the fluidic nanogenerator could be readily enhanced through a series connection. As shown in Figure 4b, a stable output voltage of 1.8 V could be achieved by connecting eight composited fibers to adapt to a broad range of applications. In a typical application scenario, a commercial capacitor was connected with the fluidic nanogenerators and could be charged up to 2.6 V (10  $\mu$ F) within 10 s or 2 V (100  $\mu$ F) within 100 s. In addition, the fluidic nanogenerators could power a series of commercial electronics like an LED lighthouse (Figures 4d, S15), indicating its good potential as a convenient energy supply for miniaturized electronic devices.

In summary, a flexible fiber fluidic nanogenerator based on an aligned CNT/transition metal oxide composite film was developed. An output voltage of 0.31 V and output power of 30 mW/m<sup>2</sup> had been achieved when RuO<sub>2</sub> particles were introduced in the aligned CNT sheet to serve as active components. The charge unbalance in the electric double layer at the interface between CNT/RuO<sub>2</sub> and saline water during the insertion process led to effective electricity generation. The introduction of transition metal oxide particles may provide a new way to efficiently improve electricity generation in a hydroelectric generator. This fiber fluidic nanogenerator is promising to serve as an efficient and miniature energy supply system for many electronic devices in water environments.

## ■ ASSOCIATED CONTENT

### Supporting Information

The Supporting Information is available free of charge at <https://pubs.acs.org/doi/10.1021/acsmaterialslett.1c00392>.

Experimental details of preparation and measurement; SEM and TEM images; water contact angle images; micrographs of a water droplet flowed over a fiber nanogenerator surface; I–V curve, output voltage, current power density of fluidic nanogenerators; zeta potential curves; photographs of fluidic nanogenerators powering a model of lighthouse (PDF)  
A water droplet flowed over a fiber nanogenerator surface with a speed of  $\sim$ 1.5 cm/s (AVI)

## ■ AUTHOR INFORMATION

### Corresponding Authors

**Peining Chen** – State Key Laboratory of Molecular Engineering of Polymers, Department of Macromolecular Science and Laboratory of Advanced Materials, Fudan University, Shanghai 200438, China; Email: [peiningc@fudan.edu.cn](mailto:peiningc@fudan.edu.cn)

**Huisheng Peng** – State Key Laboratory of Molecular Engineering of Polymers, Department of Macromolecular Science and Laboratory of Advanced Materials, Fudan University, Shanghai 200438, China; [orcid.org/0000-0003-3746-8494](https://orcid.org/0000-0003-3746-8494); Email: [penghs@fudan.edu.cn](mailto:penghs@fudan.edu.cn)

### Authors

**Tiancheng Zhao** – State Key Laboratory of Molecular Engineering of Polymers, Department of Macromolecular Science and Laboratory of Advanced Materials, Fudan University, Shanghai 200438, China

**Yajie Hu** – State Key Laboratory of Molecular Engineering of Polymers, Department of Macromolecular Science and Laboratory of Advanced Materials, Fudan University, Shanghai 200438, China

**Wen Zhuang** – State Key Laboratory of Molecular Engineering of Polymers, Department of Macromolecular Science and Laboratory of Advanced Materials, Fudan University, Shanghai 200438, China

**Yifan Xu** – State Key Laboratory of Molecular Engineering of Polymers, Department of Macromolecular Science and Laboratory of Advanced Materials, Fudan University, Shanghai 200438, China

**Jianyou Feng** – State Key Laboratory of Molecular Engineering of Polymers, Department of Macromolecular Science and Laboratory of Advanced Materials, Fudan University, Shanghai 200438, China

Complete contact information is available at: <https://pubs.acs.org/10.1021/acsmaterialslett.1c00392>

### Author Contributions

The manuscript was written through contributions of all authors. All authors have given approval to the final version of the manuscript.

### Notes

The authors declare no competing financial interest.

## ■ ACKNOWLEDGMENTS

This work was supported by MOST (2016YFA0203302), NSFC (21634003, 21805044), STCSM (20JC1414902, 19QA1400800), and SHMEC (2017-01-07-00-07-E00062).

## REFERENCES

- (1) Huang, Y.; Cheng, H.; Qu, L. Emerging Materials for Water-Enabled Electricity Generation. *ACS Mater. Lett.* **2021**, *3*, 193–209.
- (2) Zhang, Z.; Li, X.; Yin, J.; Xu, Y.; Fei, W.; Xue, M.; Wang, Q.; Zhou, J.; Guo, W. Emerging hydrovoltaic technology. *Nat. Nanotechnol.* **2018**, *13*, 1109–1119.
- (3) Wang, K.; Li, J. Electricity generation from the interaction of liquid–solid interface: a review. *J. Mater. Chem. A* **2021**, *9*, 8870–8895.
- (4) Xu, Y.; Chen, P.; Peng, H. Generating Electricity from Water through Carbon Nanomaterials. *Chem. - Eur. J.* **2018**, *24*, 6287–6294.
- (5) Xu, W.; Song, Y.; Xu, R.; Wang, Z. Electrohydrodynamic and Hydroelectric Effects at the Water–Solid Interface: from Fundamentals to Applications. *Adv. Mater. Interfaces* **2021**, *8*, 2000670.
- (6) Liu, G.; Chen, T.; Xu, J.; Wang, K. Blue energy harvesting on nanostructured carbon materials. *J. Mater. Chem. A* **2018**, *6*, 18357–18377.
- (7) Ghosh, S.; Sood, A. K.; Kumar, N. Carbon Nanotube Flow Sensors. *Science* **2003**, *299*, 1042–1044.
- (8) Dhiman, P.; Yavari, F.; Mi, X.; Gullapalli, H.; Shi, Y.; Ajayan, M. P.; Koratkar, N. Harvesting energy from water flow over graphene. *Nano Lett.* **2011**, *11*, 3123–3127.
- (9) Yin, J.; Zhang, Z.; Li, X.; Zhou, J.; Guo, W. Harvesting energy from water flow over graphene? *Nano Lett.* **2012**, *12*, 1736–1741.
- (10) Kim, J.; Lee, J.; Kim, S.; Jung, W. Highly Increased Flow-Induced Power Generation on Plasmonically Carbonized Single-Walled Carbon Nanotube. *ACS Appl. Mater. Interfaces* **2016**, *8*, 29877–29882.
- (11) Yin, J.; Zhang, Z.; Li, X.; Yu, J.; Zhou, J.; Chen, Y.; Guo, W. Waving potential in graphene. *Nat. Commun.* **2014**, *5*, 3582.
- (12) Xu, Y.; Chen, P.; Zhang, J.; Xie, S.; Wan, F.; Deng, J.; Cheng, X.; Hu, Y.; Liao, M.; Wang, B.; Sun, X.; Peng, H. A One-Dimensional Fluidic Nanogenerator with a High Power Conversion Efficiency. *Angew. Chem., Int. Ed.* **2017**, *56*, 12940–12945.
- (13) Zhen, Z.; Li, Z.; Zhao, X.; He, Y.; Zhong, Y.; Huang, M.; Wang, M.; Zhu, H. A wrinkled graphene and ionic liquid based electric generator for the sea energy harvesting. *2D Mater.* **2019**, *6*, 045040.
- (14) Yin, J.; Li, X.; Yu, J.; Zhang, Z.; Zhou, J.; Guo, W. Generating electricity by moving a droplet of ionic liquid along graphene. *Nat. Nanotechnol.* **2014**, *9*, 378–383.
- (15) Liu, R.; Liu, C.; Fan, S. Hydrocapacitor for Harvesting and Storing Energy from Water Movement. *ACS Appl. Mater. Interfaces* **2018**, *10*, 35273–35280.
- (16) Zhen, Z.; Li, Z.; Zhao, X.; Zhong, Y.; Huang, M.; Zhu, H. A non-covalent cation- $\pi$  interaction-based humidity-driven electric nanogenerator prepared with salt decorated wrinkled graphene. *Nano Energy* **2019**, *62*, 189–196.
- (17) Zhao, F.; Liang, Y.; Cheng, H.; Jiang, L.; Qu, L. Highly efficient moisture-enabled electricity generation from graphene oxide frameworks. *Energy Environ. Sci.* **2016**, *9*, 912–916.
- (18) Jian, Z.; Liu, P.; Li, F.; He, P.; Guo, X.; Chen, M.; Zhou, H. Core-shell-structured CNT@RuO<sub>2</sub> composite as a high-performance cathode catalyst for rechargeable Li–O<sub>2</sub> batteries. *Angew. Chem., Int. Ed.* **2014**, *53*, 442–446.
- (19) Yang, J.; Yang, Z.; Li, L. H.; Cai, Q.; Nie, H.; Ge, M.; Chen, X.; Chen, Y.; Huang, S. Highly efficient oxygen evolution from CoS<sub>2</sub>/CNT nanocomposites via a one-step electrochemical deposition and dissolution method. *Nanoscale* **2017**, *9*, 6886–6894.
- (20) Xu, J.-J.; Chang, Z.-W.; Wang, Y.; Liu, D.-P.; Zhang, Y.; Zhang, X.-B. Cathode Surface-Induced, Solvation-Mediated, Micrometer-Sized Li<sub>2</sub>O<sub>2</sub> Cycling for Li–O<sub>2</sub> Batteries. *Adv. Mater.* **2016**, *28*, 9620–9628.
- (21) Shin, H.-S.; Seo, G. W.; Kwon, K.; Jung, K.-N.; Lee, S. I.; Choi, E.; Kim, H.; Hwang, J.-H.; Lee, J.-W. A combined approach for high-performance Li–O<sub>2</sub> batteries: A binder-free carbon electrode and atomic layer deposition of RuO<sub>2</sub> as an inhibitor–promoter. *APL Mater.* **2018**, *6*, 047702.
- (22) Fang, H. T.; Liu, M.; Wang, D.; Ren, D.; Sun, X. Fabrication and supercapacitive properties of a thick electrode of carbon nanotube–RuO<sub>2</sub> core–shell hybrid material with a high RuO<sub>2</sub> loading. *Nano Energy* **2013**, *2*, 1232–1241.
- (23) Lo, A. Y.; Jheng, Y.; Huang, T. C.; Tseng, C. Study on RuO<sub>2</sub>/CMK-3/CNTs composites for high power and high energy density supercapacitor. *Appl. Energy* **2015**, *153*, 15–21.
- (24) Wang, P.; Xu, Y.; Liu, H.; Chen, Y.; Yang, J.; Tan, Q. Carbon/carbon nanotube-supported RuO<sub>2</sub> nanoparticles with a hollow interior as excellent electrode materials for supercapacitors. *Nano Energy* **2015**, *15*, 116–124.
- (25) Wang, X.; Yin, Y.; Hao, C.; You, Z. A high-performance three-dimensional micro supercapacitor based on ripple-like ruthenium oxide–carbon nanotube composite films. *Carbon* **2015**, *82*, 436–445.
- (26) Kong, S.; Cheng, K.; Ouyang, T.; Gao, Y.; Ye, K.; Wang, G.; Cao, D. Facile electrodeposition processed of RuO<sub>2</sub>–graphene nanosheets–CNT composites as a binder-free electrode for electrochemical supercapacitors. *Electrochim. Acta* **2017**, *246*, 433–442.
- (27) Yin, Y.; Wang, X.; You, Z. Integration of Ruthenium oxide–Carbon Nanotube Composites with Three-Dimensional Interdigitated Microelectrodes for the Creation of On-Chip Supercapacitors. *Int. J. Electrochem. Sci.* **2017**, *12*, 3883–3906.
- (28) Lin, Y. S.; Lee, K. Y.; Chen, K. Y.; Huang, Y. Superior capacitive characteristics of RuO<sub>2</sub> nanorods grown on carbon nanotubes. *Appl. Surf. Sci.* **2009**, *256*, 1042–1045.
- (29) He, S.; Zhang, Y.; Qiu, L.; Zhang, L.; Xie, Y.; Pan, J.; Chen, P.; Wang, B.; Xu, X.; Hu, Y.; Dinh, C. T.; De Luna, P.; Banis, M. N.; Wang, Z.; Sham, T.-K.; Gong, X.; Zhang, B.; Peng, H.; Sargent, E. H. Chemical-to-Electricity Carbon: Water Device. *Adv. Mater.* **2018**, *30*, 1707635.
- (30) Kim, S. H.; Haines, C. S.; Li, N.; Kim, K. J.; Mun, J. T.; Choi, C.; Di, J.; Oh, Y. J.; Oviedo, J. P.; Bykova, J.; Fang, S.; Jiang, N.; Liu, Z.; Wang, R.; Kumar, P.; Qiao, R.; Priya, S.; Cho, K.; Kim, M.; Lucas, M. S.; Drummy, L. F.; Maruyama, B.; Lee, D. Y.; Lepró, X.; Gao, E.; Albarq, D.; Ovalle-Robles, R.; Kim, S. J.; Baughman, R. H. Harvesting electrical energy from carbon nanotube yarn twist. *Science* **2017**, *357*, 773–778.



ACS IN FOCUS

Cellular Agriculture  
Lab-Grown  
Dilek Erilliç-D  
Dorothee E

Machine Learning in Chemistry  
Jon Paul Janet &  
Heather J. Kulik

bacterials  
Toria Cheng Jaramillo  
William M. Wuest

ACS In Focus ebooks are digital publications that help readers of all levels accelerate their fundamental understanding of emerging topics and techniques from across the sciences.

pubs.acs.org/series/infocus

ACS Publications  
Most Trusted. Most Cited. Most Read.

QR code